

Primljen / Received: 19.5.2015.

Ispravljen / Corrected: 18.1.2016.

Prihvaćen / Accepted: 18.3.2016.

Dostupno online / Available online: 10.9.2016.

Preliminary study on the influence of fibre orientation in fibre reinforced mortars

Authors:



Julien Michels, PhD. CE
Swiss Federal Laboratories for Materials
Science and Technology - EMPA
julien.michels@empa.ch



Assist.Prof. **Matija Gams**, PhD. CE
Slovenian National Building Institute
matija.gams@zag.si

Preliminary report

Julien Michels, Matija Gams

Preliminary study on the influence of fibre orientation in fibre reinforced mortars

The influence of steel fibres in fibre reinforced mortars is considered in the paper. Fresh mortar samples with randomly distributed fibres are placed in a spiral coil and exposed to electromagnetic field so as to achieve orientation of fibres. The location and orientation of fibres is defined by x-ray images. The bending strength testing with deflection checking using the ICS system (Digital Image Correlation System) is conducted. Considering the fibre orientation and load applied, the results exhibit better energy dissipation and greater energy at fracture in case of samples with oriented fibres.

Ključne riječi:

concrete manufacturing and technology, concrete structures, strength, material testing

Prethodno priopćenje

Julien Michels, Matija Gams

Preliminarno istraživanje utjecaja orijentacije vlakana u mikroarmiranim mortovima

U radu se obrađuje utjecaj čeličnih vlakana u mikroarmiranim mortovima. Uzorci morta u svježem stanju, s nasumično raspoređenim vlaknima su smješteni u spiralnu zavojnicu i izloženi elektromagnetskom polju u cilju postizanja usmjerenosti vlakana. Lokacija i orijentacija vlakana je određena rendgenskom snimkom. Provedena su ispitivanja čvrstoće na savijanje uz kontrolu progiba ISC sustavom (engl. *Digital Image Correlation System - ICS*). S obzirom na orijentaciju vlakana, rezultati su pokazali poboljšanu disipaciju energije i veću energiju pri lomu kod uzoraka s usmjerenim vlaknima.

Ključne riječi:

proizvodnja i tehnologija betona, betonske konstrukcije, čvrstoća, ispitivanje materijala

Vorherige Mitteilung

Julien Michels, Matija Gams

Vorläufige Untersuchung zum Einfluss der Faserorientierung in mikroarmierten Mörteln

In dieser Arbeit wird der Einfluss von Stahlfasern in mikroarmierten Mörteln untersucht. Mörtelproben in frischem Zustand mit zufällig angeordneten Fasern wurden in eine Spiralspule gelegt und einem Elektromagnetfeld ausgesetzt, um die Fasern auszurichten. Lage und Ausrichtung der Fasern wurden mit Röntgenaufnahmen ermittelt. Prüfungen zur Biegefestigkeit einschliesslich Kontrolle der Verformungen mittels ISC System (engl. *Digital Image Correlation System - ICS*) wurden durchgeführt. In Bezug auf die Ausrichtung der Fasern und die erzielten Spannungen haben die Resultate bei den Proben mit ausgerichteten Fasern eine verbesserte Energiedissipation und erhöhte Energie beim Versagen nach der Entwicklung von Rissen gezeigt.

Ključne riječi:

Betonherstellung und Betontechnologie, Betonkonstruktionen, Festigkeit, Materialuntersuchungen

1. Introduction

Advantages of a smeared fibre reinforcement in a cement or concrete conglomerate are nowadays well known, and have been documented in a multitude of publications over the past few decades. A good overview on the evolution of fibres as a concrete reinforcement is given in [1]. The main change caused by adding fibres to a cement mixture is the transformation from a quasi-brittle to a pseudo-ductile material, since the additional reinforcement allows transfer of tensile stresses even at large crack openings. The parameters with the strongest influence on the improved tensile capacity compared to plain cement or concrete are the fibre mass or volume content (usually expressed in $[\text{kg}/\text{m}^3]$ or $[\%]$, respectively), fibre aspect ratio (length-to-diameter-ratio), bond efficiency of the embedded fibre(s), and the fibre orientation with respect to the direction of the applied stress. A higher fibre content and higher aspect ratio generally lead to a higher post cracking strength [2-11]. On the other hand, the bond characteristics of the embedded fibres are determined by the fibre geometry and surface adhesion [12, 13]. Finally, in a concrete element loaded primarily in bending, a single fibre is the most efficient when it is aligned with the induced tensile stress. However, simple adding of fibres to the fresh concrete mixture generally leads to a random distribution and orientation in the matrix, resulting in a non-optimal fibre orientation when a specific loading scheme is considered. From a qualitative point of view, when considered as bending reinforcement in a beam, fibres are the most efficient if they are oriented horizontally. The random fibre orientation itself is influenced to a certain extent by the construction element, formwork geometry, and formwork dimensions with respect to fibre dimensions [14-17], as well as by the casting direction. For instance, research presented in [18] has revealed differences in the post-cracking tensile strength of the steel fibre reinforced concrete for drill cones taken out of a previously cast plate element from different directions. Scaling effects when testing small-scale laboratory bending beams, or investigating large-scale plate elements with variable height, are presented in [4].

One example of an attempt to deliberately influence fibre orientation is documented in a US patent from 2004 [19], in which a magnetic device is used to orient steel fibres during the casting process. In the present work, the fibres were oriented in relatively small samples. For this purpose, the prisms were placed into a helical coil in which an electro-magnetic field was induced. X-ray photos [20] were taken to obtain a visual proof of the changed fibre orientation. Eventually, the small bending elements were statically tested. The aim of the paper is to quantitatively assess the effect of orientation, which could be subsequently used in a cost-benefit analysis to optimize construction of precast elements by reducing the amount of fibres. It is acknowledged that the used geometry is clearly smaller than the conventional laboratory-scale specimens used in the steel fibre reinforced concrete characterization. This implies that the results in terms of post-cracking strength should be considered in a qualitative rather than quantitative manner. The primary aim of the current study was to experimentally verify technical feasibility of a deliberate fibre orientation in cementitious

materials, and conditions required to achieve it. Secondly, experimental investigation was used to study the effect of oriented fibres compared to randomly distributed fibres.

2. Materials, samples and methods

2.1. Materials

It was not possible to use a regular concrete composition because of the small size of the formwork. Therefore, a ready mix mortar [21] with aggregate size up to 3 mm was used. No specific grain size distribution design was performed for the present investigation. According to the manufacturer, compressive strength is higher than 5 MPa after 28 days [21]. Commercially available hooked steel fibres (Figure 1) were used as reinforcement. The fibres are 30 mm in length and 0.6 mm in diameter, and thus the aspect ratio (λ_f) is 50. The declared tensile strength of the fibres is 1200 MPa (Data Sheet [22]).



Figure 1. Steel fibres

2.2. Samples

The size of the prismatic samples was 37 mm x 36 mm in cross section (width x height), and they had a small necking at the top (of about 3 mm x 3 mm) due to the shape of the plastic moulds used as formwork.

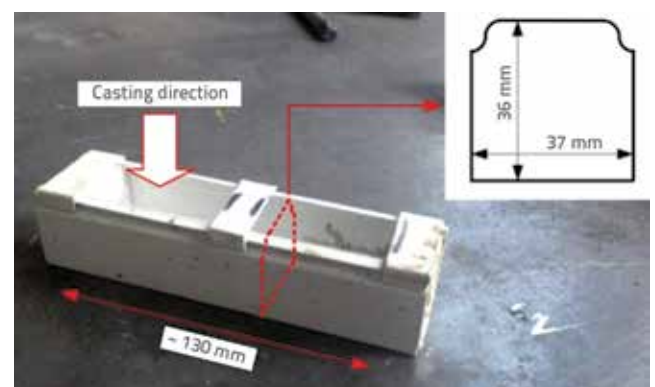


Figure 2. Formwork and cross section of samples

The choice of such moulds was a deliberate decision, because a large number of specimens had to be cast in a simple way. Furthermore, the later presented coil had a limited size, which put

another constraint on the specimen dimensions. A photograph of the formwork and the sample is shown in Figure 2. Each sample was approximately 130 mm in total length. A constant span L of 100 mm was used in the three-point bending tests.

Two mass contents (M_f), i.e. 30 and 40 kg/m³, were used for specimen fabrication. This corresponds to the volume fractions of 0.39 % and 0.52 %, respectively. Both random and deliberate fibre orientation were considered for the two mass contents. The prescribed quantity of water was added to the dry mortar mix and mixed. All samples were prepared with the same batch of mortar. Table 1 summarizes the labelling, number of specimens, and characteristics of each series.

Table 1. Test series configurations

Series	No. of specimens	Fibre content [kg/m ³]	Fibre orientation
30-RD	6	30	random
30-OR	6	30	oriented
40-RD	6	40	random
40-OR	7	40	oriented

2.3. Fibre orientation and modelling

The present subsection explains the orienting technique with the electromagnetic coil, the subsequent X-ray photography, and the procedure for obtaining fibre positions and orientations. The reader is also invited to consult literature on the computer-tomography based evaluation of fibre dispersion and orientation in concrete mixtures [23, 24].

The computed tomography (CT) is a computer-processed reconstruction of a tomographic plane. It is an X-ray imaging method for displaying a layered representation of an examined part of a body, in which the ionising radiation is used for image generation.

2.3.1. Fibre orienting technique

Samples designated for orientation (30-OR and 40-OR) were placed into an electromagnetic coil (Figure 3). The coil with the sample inside was placed on a slump test flow table. Once the DC current was run through the coil, the table was dropped 10 times in 10 seconds. After this, the current was stopped and the samples removed from the coil, placed in a hermetically sealed plastic bag, and left to cure. The fibre orienting procedure is heuristic and was obtained by tests using dry sand and fibre mixtures. The electromagnetic coil was custom-built for this research. It has a hollow rectangular 4 x 4 cm core, and is 20 cm in length. It consists of 100 turns of rectangular 8 x 5 mm copper wire. The current used for preparing samples amounted to approximately 220 A, which generated the magnetic field strength of 134.2 mT. This was measured using a Hall probe. The current intensity was based on initial successful trials on dry sand mixtures. The distribution of the field strength in longitudinal (B_x)

as well as in both transversal directions (B_y, B_z), under the current of 50 A, is given in Figure 4 for demonstration purposes. The strongest intensity was registered in the central part of the coil, whereas a decrease towards both ends can be observed.

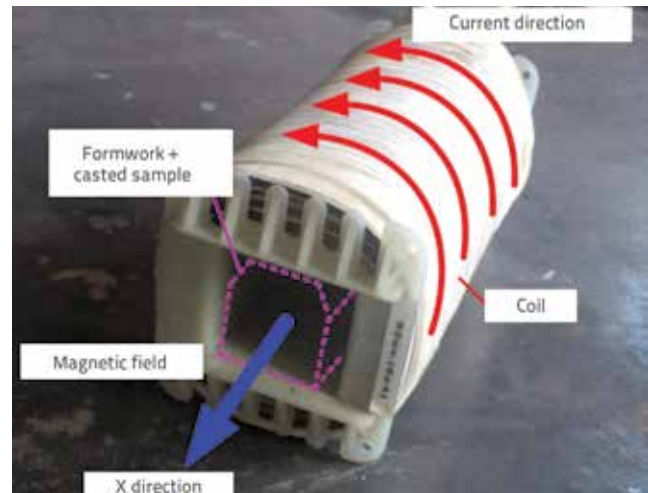


Figure 3. Custom built electromagnetic coil

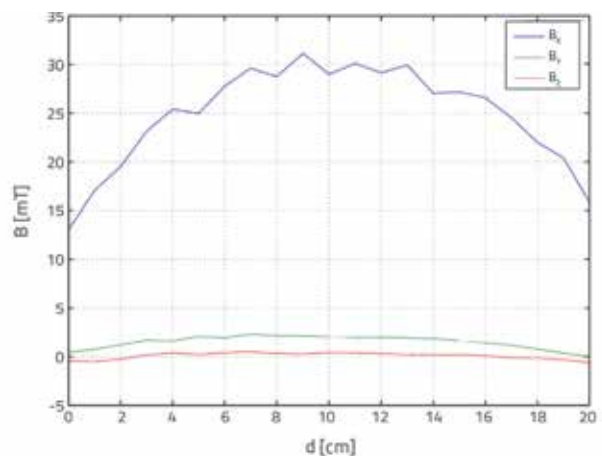


Figure 4. Magnetic field values B_x, B_y and B_z [mT] in three directions, longitudinal (x) and transversal (y,z) under the current of 50 A

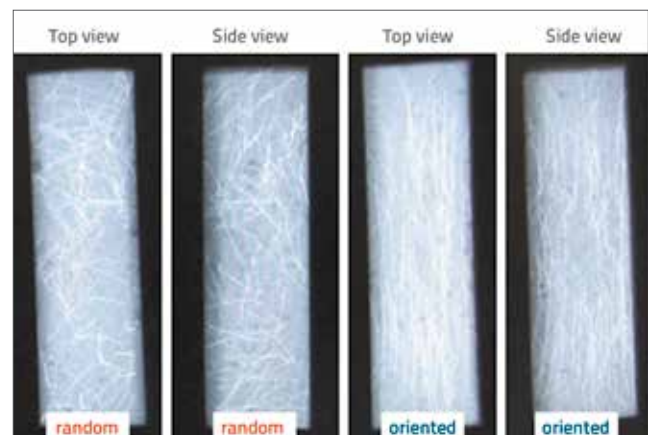


Figure 5. Top and side X-ray photo of prisms with random and oriented fibres

2.3.2. X-ray photography

Prisms were taken to an X-ray machine in order to determine the orientation of fibres in the hardened concrete samples. A medical X-ray device was used to take pictures of samples from the side and from the top. These pictures already revealed significant differences between the randomly placed and oriented fibres, as can clearly be observed in Figure 5.

2.3.3. Calculation of 3D fibre positions

In order to mathematically describe the orientation of fibres inside the samples, X-ray photos were first digitalized and processed so as to maximize the contrast between the fibres and concrete. Digital images were then scaled to real dimensions. This scaling was accurate and simple because reference standards (etalons) were positioned next to the samples on each X-ray image. Once scaled, vector lines were drawn manually over the X-ray images of fibres. High fibre concentrations or small fibre projections were observed at some places and, in such cases, individual fibres had to be identified based on the analyst's decision. Some errors might have occurred due to the very nature of this procedure. However, the extent of such errors is such that they can not have a strong effect on the overall picture. Additionally, the size of specimens and the density of fibres were chosen in such a way to limit the frequency of errors. Because pictures of each sample from the top as well as from the side were available, 3D locations of the fibres inside the samples could be determined. In this phase, the crucial part was to find the correct pairs of projections. In order to do this, a simple computer program was written, which compared the locations of midpoints of the projections. The nearest ones were chosen as pairs, with the following natural restrictions: each projection could only be used once and the maximum allowed distance between midpoints of the projections was 10 mm. If the projections were without any errors, the program would find (correct) pairs for all fibres. But, due to the reasons explained above, it was impossible to establish pairs for some projections. An average number of projections without a pair amounted to approximately 10%.

2.4. Three-point bending test setup

The 3-point-bending tests were carried out at the laboratory of the Slovenian National Building and Civil Engineering Institute (ZAG). A photo of the setup is given in Figure 6. The specimens were loaded under the controlled displacement conditions by means of a hydraulic jack, at the rate of 1 mm/min. The span L amounted to 100 mm in every test. The displacements were recorded by means of a digital image correlation system (ICS). Both cameras of the system are also shown in Figure 6. This technique allows in-plane and out-of-plane recording of displacements for a measuring field previously defined by means of an irregular contrast pattern, [25, 26].

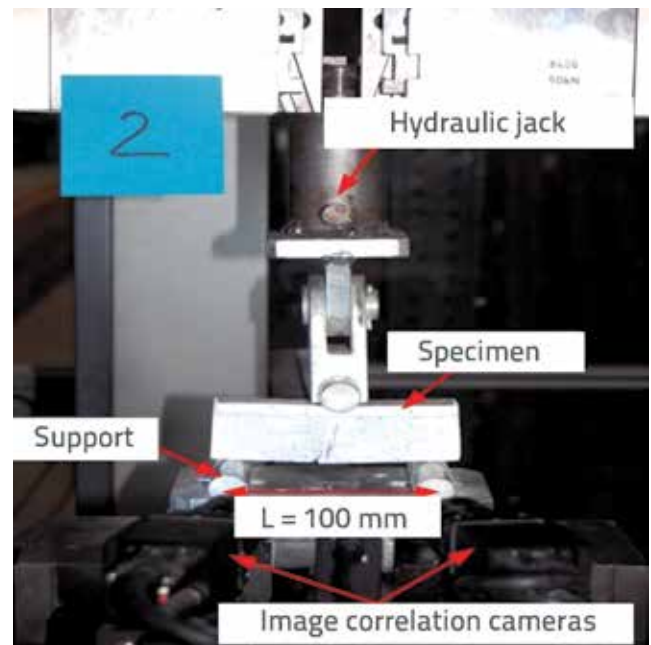


Figure 6. Test setup for 3-point bending tests

2.5. Experimental and numerical assessment of CMOD

The maximum crack width or the crack mouth opening displacement (CMOD) is a very important structural parameter in research, and also in practical structural design. It is of key importance when durability issues are investigated. This section presents a comparison between an experimental and a numerical approach for the assessment of the CMOD. From an experimental point of view, the ICS measurements allow for a simple evaluation by continuously monitoring relative displacement between two points at the crack tip, as presented in Figure 7.

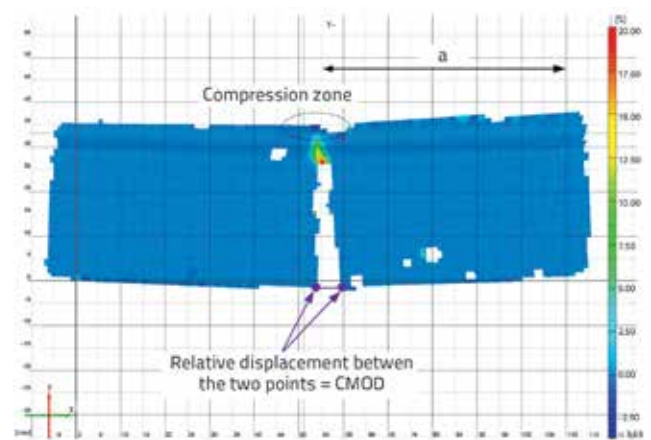


Figure 7. CMOD assessment via Image Correlation System

A simplified geometric approach for the CMOD derivation through the hinge rotation and the compression zone height is presented below. A comparison between the solution based

on the inverse analysis and the direct assessment with the Image Correlation measurements is presented in the Chapter 3. section. Both angular rotations (see Figure 8) can be evaluated using the respective vertical displacements:

$$\psi_1 = \frac{\delta}{L/2} \tag{1}$$

$$\psi_2 = \frac{\delta_r}{\alpha} \tag{2}$$

Since

$$\frac{\delta}{L} = \frac{\delta_r}{L-a} \tag{3}$$

$$\delta_r = 2 \cdot \delta \cdot \frac{L-a}{L} \tag{4}$$

and since

$$\theta = \Psi_1 + \Psi_2 \tag{5}$$

the hinge rotation can be rewritten as:

$$\theta = \frac{2 \cdot \delta}{L} \cdot \left(\frac{L-a}{L} + 1 \right) = \frac{2 \cdot \delta}{\alpha} \tag{6}$$

In the cross section with a height h , the hinge rotation can be linked to the crack mouth opening displacement CMOD, and the height of the compression zone x_c , using the geometric relations presented in Figure 8:

$$\theta = \frac{CMOD}{h - x_c} \tag{7}$$

The exact position of x_c can be obtained by the cross-section analysis as presented in [4]. This inverse analysis fits material parameters of an exponentially decreasing constitutive (σ - ε) - law in tension:

$$\sigma(\varepsilon) = f_{pc} \cdot e^{-\beta(\varepsilon_t - \varepsilon_{ct})} \tag{8}$$

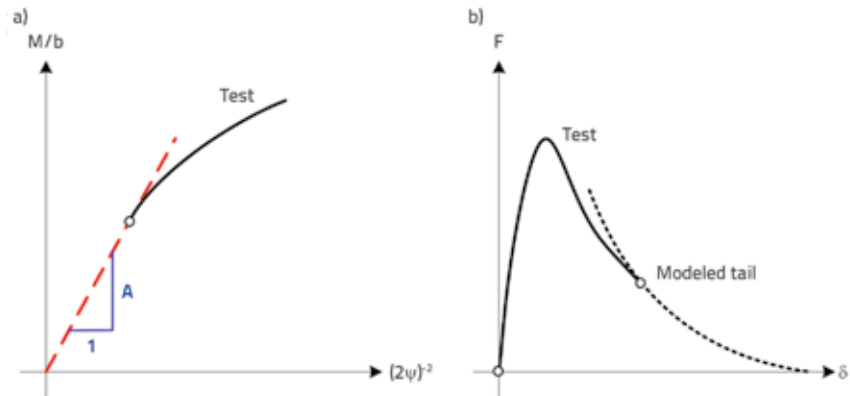


Figure 9. Schematic representation of a) M/b Vs. $(2\psi)^2$ curve, and b) modelled tail up to zero force

for which f_{pc} represents the immediate post-cracking strength after occurrence of the first crack and ε_{ct} the cracking tensile strain. The algorithm postulates the presented hinge-rotation crack pattern (see Figure 8, hinge location a is known from the experiment), and subsequently adapts the parameters f_{pc} and β until a best fit to the experimental results is obtained [4]. It is mentioned that for a loading step, the height of the compression zone, is known due to the equilibrium between the tensile and compressive forces in the cross-section. Since θ can be derived from the deflection level and the crack position a , the crack opening CMOD can be calculated from Eq. 8.

2.6. Numerical derivation of fracture energy

Fracture energy is generally defined as the area under the tensile stress-crack opening curve, the maximum value being reached when the zero tensile stress is transferred through the crack opening. An alternative possibility for calculating it is the following procedure via the energy dissipation W (area under the force-deflection curve):

$$G_r = \frac{W}{b \cdot h} \tag{9}$$

The product $b \cdot h$ is equivalent to the cross section, fully cracked at the end. For the sake of simplicity, the cross section is considered to be rectangular, and it measures 37 mm in width and 36 mm in

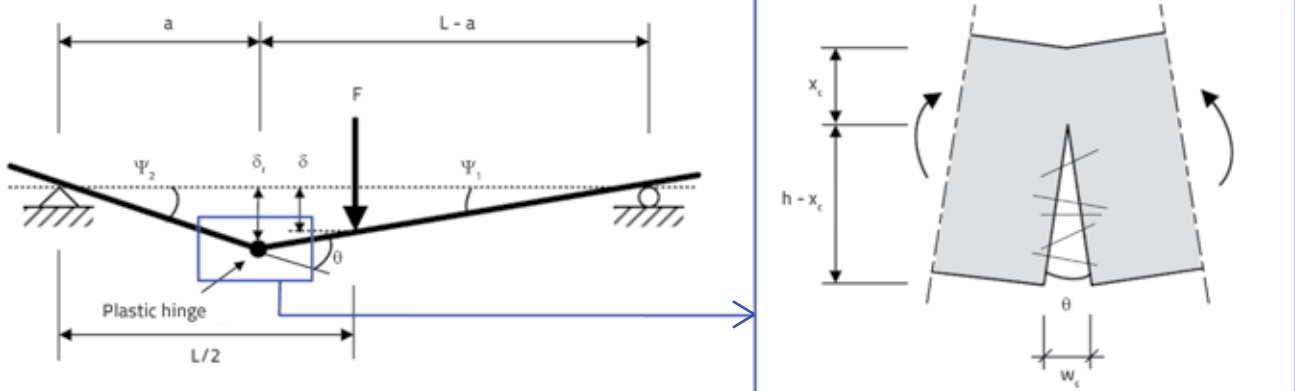


Figure 8. Crack pattern and hinge rotation for 3-point bending tests

height. In order to determine the total fracture energy, it would be necessary to run each test until no force is transmitted through the cross-section. The energy dissipation until complete fracture of the samples is not available for any of the previously presented results. An extrapolation technique shown in [27] (based on an earlier work of Bažant [28] and others [29, 30]) is used to derive the full work capacity from available test results. The method is based on determination of the softening parameter A, which defines the shape of the softening curve. This parameter can be obtained by plotting the bearing moment over the sample width M/b against $(2\Psi)^2$, as it corresponds to the initial slope of the curve. A schematic representation is given in Figure 9. Residual forces after the last measured value are subsequently derived by:

$$F_{tail} = \frac{b \cdot L \cdot A}{4 \cdot \delta} \tag{10}$$

The angular rotation ψ , taken to be equal to the angular rotation as shown in Figure 8, is subsequently evaluated for the related deflection at the hinge location. Finally, the results in terms of mid-span deflection are transformed according to the relative geometric relations (Figure 8). The exact crack location can be directly obtained through the Image Correlation measurements. An example for derivation of the softening parameter A is given in Figure 10.

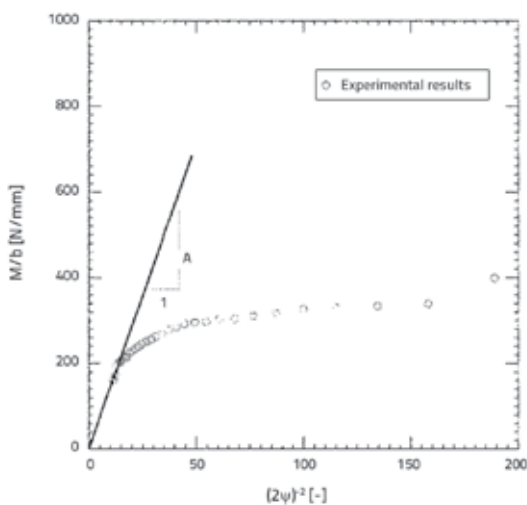


Figure 10. Softening parameter derivation example for prisms with 40 kg/m³ (nasumična raspodjela vlakana)

The test data shown in the figure are derived from the specimen with the fibre mass content of 40 kg/m³ and with a random fibre distribution. The range for which the linear trend line is established is eventually dependent on the deliberate human decision after visual inspection of the curve [27].

3. Results and discussion

3.1. Test results

Even though the test setup and samples are not fully compliant with several testing recommendations for SFRC, [31-33], the

deflection at mid-span is similarly evaluated as the relative displacement between the top concrete surface and the horizontal axis at half of the specimen height (Figure 11).

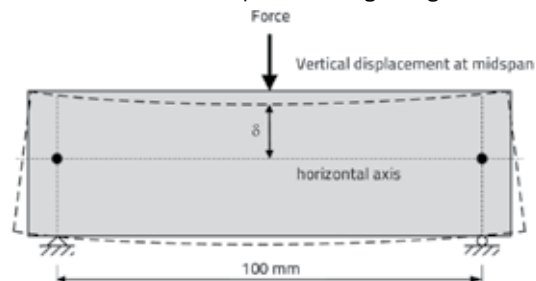


Figure 11. Definition of mid-span deflection

It could be observed for all specimens that a single crack opening occurs, and that energy dissipation is concentrated at one plastic hinge. As an example, Figure 12 shows strain evolution in horizontal direction for four consecutive force levels for a specimen with 40 kg/m³ of randomly oriented fibres. Force-mid-span deflection curves (up to 2 mm) are given in Figure 13. Maximum forces F_u for the respective fibre contents of 30 and 40 kg/m³ are presented in Figure 14 and Table 2.

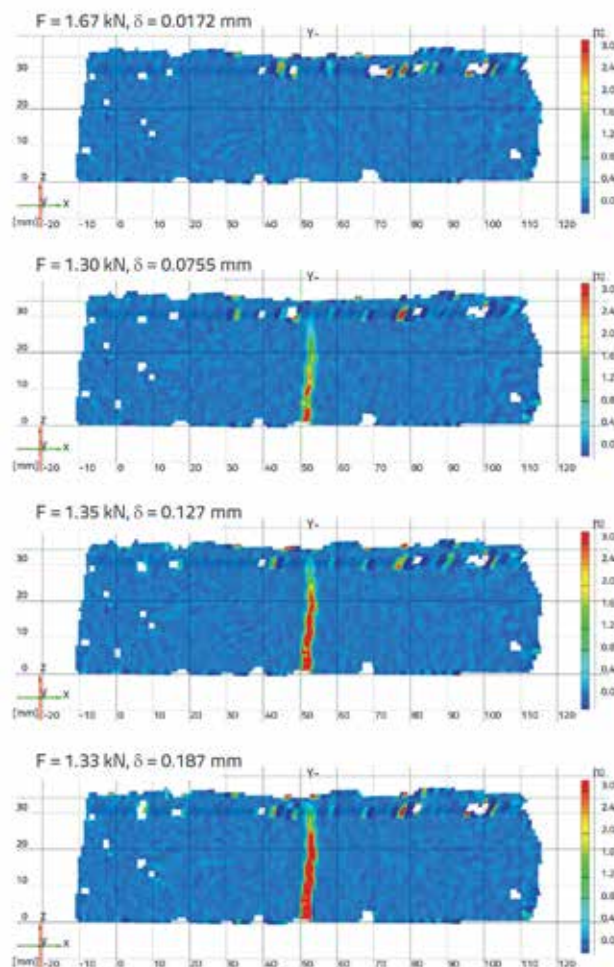


Figure 12. Tensile strains in x-directions of four consecutive load (displacement) steps, taken with Image Correlation Systems for specimen with 40 kg/m³ of randomly distributed steel fibres

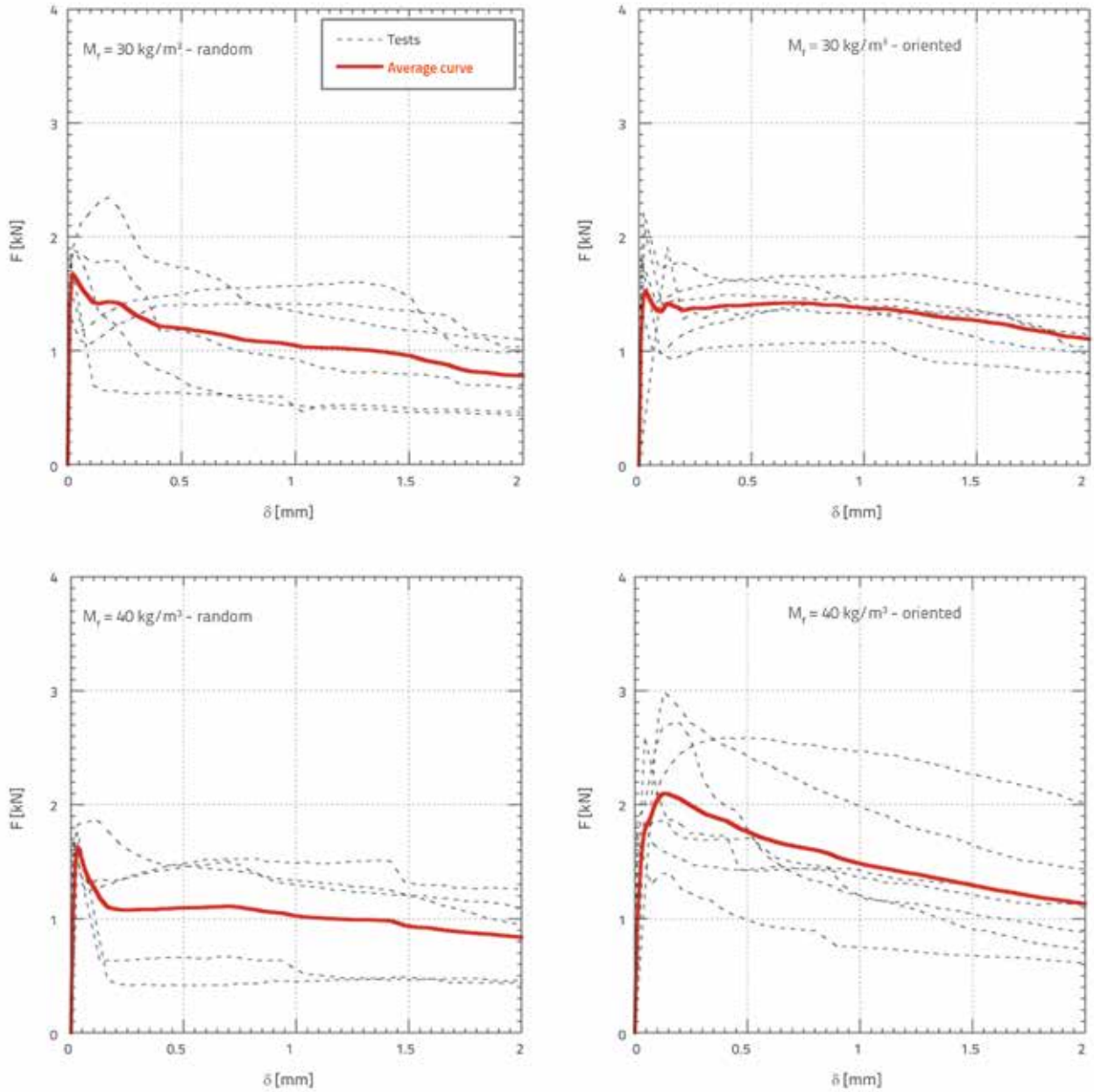


Figure 13. Force-mid-span deflection curves for both fibre contents and orientation categories

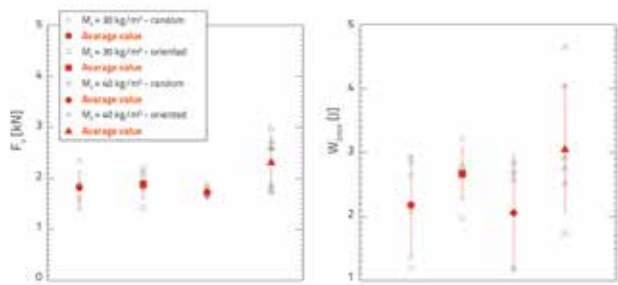


Figure 14. Ultimate forces F_u and energy dissipation W_{2mm} up to 2mm mid-span deflection for both fibre contents and orientation categories

Table 2. Summary of all tested prisms - ultimate load and energy dissipation up to 2 mm of mid-span deflection

Specimen	F_u [kN]	W_{2mm} [J]
30-RD	1,82 (+/-0,31)	2,18 (+/-0,75)
30-OR	1,88 (+/-0,27)	2,67 (+/-0,40)
40-RD	1,73 (+/-0,09)	2,06 (+/-0,89)
40-OR	2,33 (+/-0,52)	2,33 (+/-0,98)

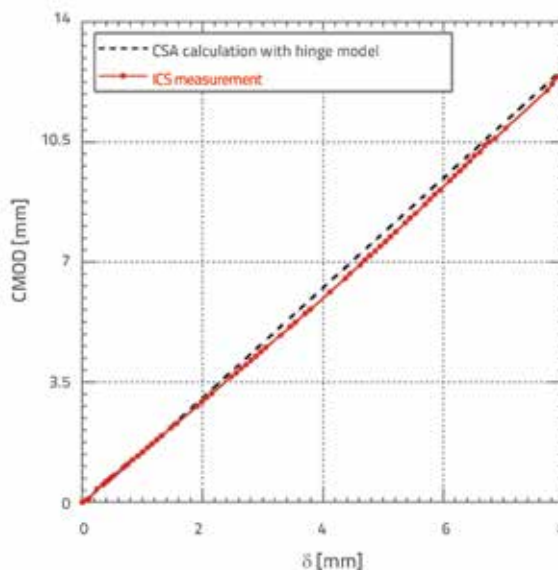
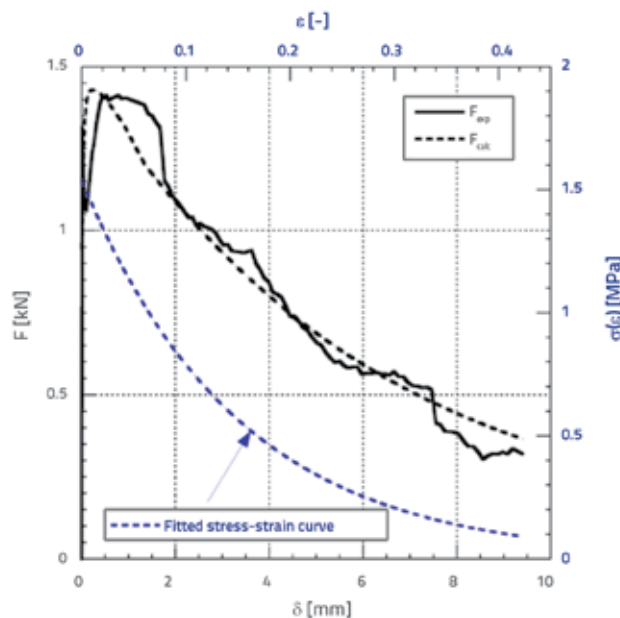


Figure 15. Experimental and fitted results (left) and comparison between derived and measured CMOD with growing deflection (right)

3.2. Experimental and numerical CMOD comparison

A comparison between the numerical and experimental force-deflection ((F – δ) curves) together with the fitted stress-strain law in tension, is given in Figure 15 for one specimen with a mass content of 30 kg/m³ and a deliberate fibre orientation. Additionally, the derived CMOD (see Section 2.5) are compared to experimental ICS measurements.

3.3. Calculated fracture energies

The derived fracture energies for all tested specimens are presented in Figure 16.

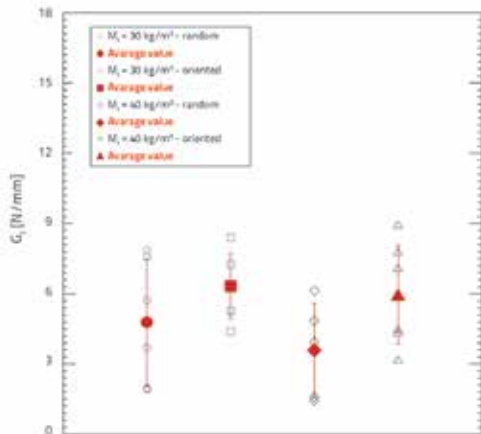


Figure 16. Derived fracture energy G_f for all samples

3.4. Fibre presence and orientation in cracked sections

The 3D-plot given in Figure 17 shows the fibre distribution and orientation with a random and a deliberate orientation in case of a

mass content of 40 kg/m³. The effect of magnetic field is obvious even after visual inspection. Oriented fibres are almost parallel to the horizontal axis compared to a more random 3D orientation.

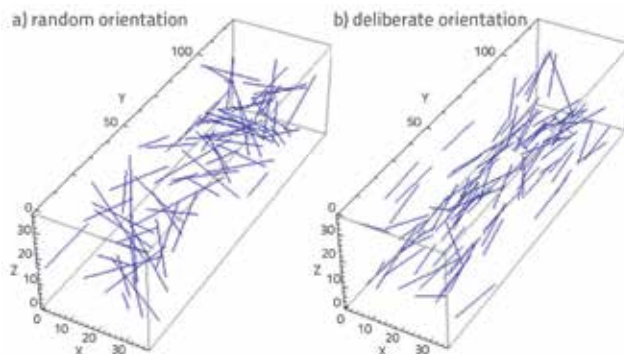


Figure 17. 3D-plot in Mathematica in case of mass content of 40 kg/m³: a) random and b) deliberate orientation

The total number of fibres in the respective cracked sections, and the related average angle of the fibres (average angle per specimen), are shown in Figure 18 in relation to the horizontal axis. Additionally, average values of each series are given in Table 3.

Table 3. Average values per series of total number of fibres and fibre orientation angle in cracked section

Specimen	$N_{f,cr,avg} (\pm s.d.)$	$\alpha_{f,cr,avg}$
30-RD	8 (± 4.4)	35,3
30-OR	9 (± 3.5)	9
40-RD	6,8 (± 2.7)	37,6
40-OR	10,6 (± 2.2)	8,4

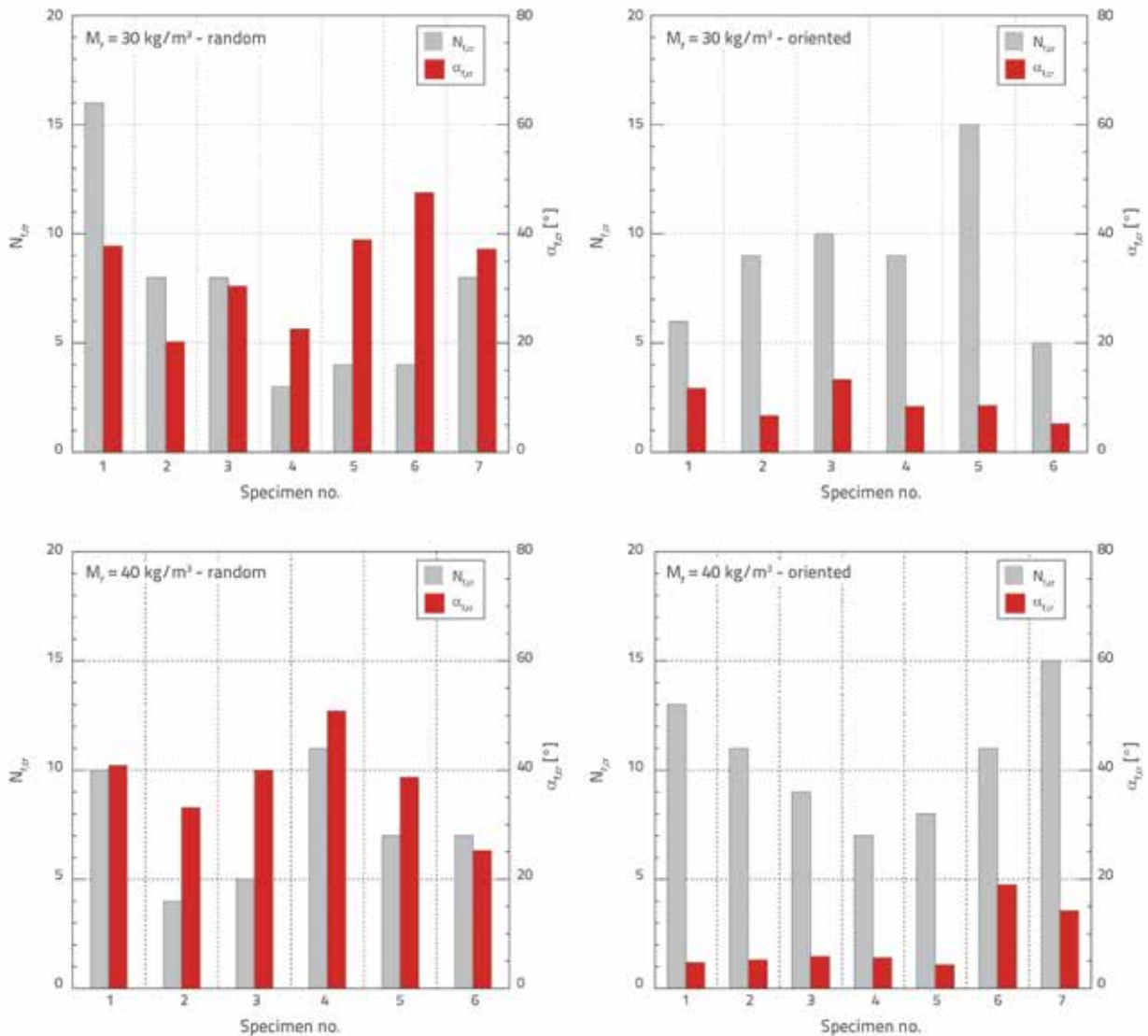


Figure 18. Number of fibres $N_{f,cr}$ and average fibre angle $\alpha_{f,cr}$ in cracked section

3.5. Discussion

The effect of oriented fibres on the bending strength of samples is not significant in case of low fibre density (30 kg/m^3), but this effect is significant in the case of higher fibre content (40 kg/m^3). An average increase of ultimate force from 1.73 in case of random orientation to 2.33 kN in case of oriented fibres can be observed (Figure 14.a), it can be concluded that the relative differences between the values remain small when standard deviations are taken into account.

An analysis of force-displacement diagrams presented in Figure 13 leads to several observations. Firstly, it can be seen from visual examination that the response of all samples is pseudo-ductile with a clearly pronounced post-peak bearing capacity, and that category 40OR (higher fibre content and deliberate fibre orientation) leads to a more pronounced hardening effect after the first crack compared to other categories.

Secondly, the effect of deliberate orientation can be assessed from a closer analysis of the evolution of the post-cracking force-deflection curve. For the category with 30 kg/m^3 (Figure 13.a and 13.b), the force drop after the peak load is less pronounced for oriented fibres than for random fibre orientation, and it eventually results in an almost horizontal plateau up to a 1 mm deflection at mid-span. The same but even more pronounced phenomenon can be observed for a fibre content of 40 kg/m^3 (Figure 13.c and 13.d). For an identical deflection value, the corresponding forces are obviously higher when oriented fibres are in charge of crack bridging.

Quantitatively, this phenomenon can be better explained with the respective energy dissipation W , corresponding to the area under the force-deflection curve. Up to a mid-span deflection of 2 mm, the values $W_{2\text{mm}}$ are summarized in Figure 14 b) and Table 2. In both fibre content categories, the deliberate fibre orientation leads to a higher energy dissipation in cracked section. For

instance, a relative average improvement of 22 and 50 % can be noticed for a fibre dosage V_f of 30 and 40 kg/m³, respectively. Similar observations can be made for fracture energy. For both fibre content categories, higher fracture energies are obtained when a deliberate fibre orientation is considered. As the fracture energy is defined by the area under the stress-crack opening curve, this observation is a logical consequence of higher fibre efficiency with fibre orientation parallel to the stress direction.

Surprisingly, a comparison between the two volume fractions with a random fibre orientation does not reveal any difference. In fact, the tests on samples with a fibre content of 40 kg/m³ reveal even lower energy dissipation than the ones with 30 kg/m³. This is in contradiction to the generally known information that energy dissipation at cracked state increases with a growing fibre content in the matrix, [2-10]. Similarly, a higher fibre content (40 kg/m³) for both random and deliberate orientations generates lower fracture energies compared to a lower fibre content (30 kg/m³). On average, the number of fibres in a cross section should increase with a growing fibre content. However, Figure 18 and Table 3 show that the average number of fibres in the cross section is not higher when a higher fibre volume fraction is used. For the random orientation, tests with 40 kg/m³ exhibit even lower fibre presence than with 30 kg/m³. This is the main reason for the surprisingly lower values of energy dissipation and fracture energy. It is believed that the small formwork dimensions compared to the fibre geometry might not have allowed a homogeneous fibre dispersion in the bulk. This point remains the strongest argument towards additional bending tests with more appropriate beam sizes.

A deliberate orientation in case of fibre mass content of 30 kg/m³ does not significantly increase the fibre presence in the cracked section (from 8 to 9 fibres). Higher energy dissipation (Table 2) and fracture energy (Figure 16) are in this case due to a more efficient use of the fibres, which are better aligned to the actual stress direction. This can be observed in Table 3 with a clearly lower average fibre angle in relation to the specimen central axis for a deliberate orientation (relative decreases of 73 %, $\alpha_{f,cr,avg}$ of 35.3 to 9). On the other hand, for a fibre content of 40 kg/m³, more fibres are located in the cracked section in case a deliberate orientation is considered. In this case, the increase is 56 % (from 6.8 to 10.6 of fibres). Here, both the lower average orientation angle and the higher number of fibres are responsible for higher energy dissipation and fracture energy. The results might further be influenced by a generally small number of fibres in each cross section, by possible concentration of fibres at the top or bottom of the cross-section, as well as by trends in the active bond length of the fibres (shorter embedded part of the fibre that is pulled out of the mortar at the crack). The results could be improved by additional tests with bigger specimens but of identical fibre length. Finally, a large number of data can be extracted with the digital image correlation measurements (ICS) compared to other instruments such as LVDTs. For instance, the exact crack location and the precise crack propagation direction can directly be assessed in our case. Furthermore, during the entire loading

process, the CMOD can easily be registered by simply controlling the crack location and subsequently defining a length change between both crack mouth tips. The application of the numerical model presented in Section 2.5 and in [4] reveals CMOD values that match very well with experimental measurements.

It can be stated that standard deviations are high for various commented parameters, and for all content and orientation categories. Additionally, all tests were stopped at a deflection level that is far from the full specimen fracture, which is why a large part of the missing tail had to be modelled. Further tests up to large deflections should give a clearer trend in terms of 'exact' fracture energy values, while also improving confidence in the applied calculation technique for modelling the missing part of the response. To summarize, it can be concluded that the presented results constitute a visible improvement in terms of energy dissipation and fracture energy when creating a deliberate fibre orientation in the bulk with a magnetic field. However, final conclusions can not be made due to a rather high scatter of results. A very positive aspect is the clearly distinct orientation of the fibres in the magnetic field direction. It is believed that this observation can be the basis for an improved structural behavior of SFRC in future applications.

4. Conclusions and outlook

The following conclusions can be drawn from the results presented in the paper:

- The technique for obtaining a deliberate fibre orientation was very easy to apply for small samples and the feasibility has been proven. For instance, a suitable magnetic device could be developed for precast concrete elements.
- The assessment of the fibre position and orientation is in this case relatively time-consuming and not applicable on a larger scale, mainly because of the large number of fibres. Automated computer-tomography based techniques, such as those indicated in the references, could be used.
- Despite the inconsistency of lower energy dissipation and fracture energy for higher fibre content, the clear improvement in the fibre alignment after exposure to magnetic field is apparent. Experimental results show an improved structural behaviour in bending at post-cracking state with regard to energy dissipation and fracture energy when fibres are oriented. Since fibre reinforced concretes should generally fulfill the purpose of such an enhanced work capacity, the advantage is apparent and should be further investigated.
- The Digital Image Correlation delivers interesting and sufficiently accurate full-field behaviour results in terms of displacement (and strains) as well as with regard to crack location, orientation and width. Advantages over traditional usage, restricted to LVDTs only, are obvious.

Future experimental tests on the orientation of fibres should be carried out on larger samples in order to gain additional confidence in the orientating technique and, possibly, to enable application of the technique for precast concrete products.

Acknowledgements

This research work was partly sponsored by the Slovenian Research Agency under grant P2-0273. The support is gratefully acknowledged. Prof. J. Sena-Cruz (ISISE, University of Minho (Portugal)) is kindly acknowledged for his valuable

comments helping us to improve the manuscript quality. Help provided by Assoc.Prof. Samo Beguš with regard to magnetic field measurements is also gratefully acknowledged. The authors equally wish to thank the X-ray laboratory of Pulmonary Clinic in Ljubljana for permitting the use of their equipment.

REFERENCES

- [1] Naaman, A.E.: Development and evolution of tensile strain-hardening FRC composites, 7th International RILEM Symposium on Fibre Reinforced Concrete, Chennai (India), 2008.
- [2] Barros, J.A.O., Cunha, V.M.C.F., Ribeiro, A.F., Antunes, J.A.B.: Post-cracking behaviour of steel fibre reinforced concrete, *Materials and Structures/Materiaux et Constructions*, 38 (2005) 275, pp. 47-56, <http://dx.doi.org/10.1617/14058>
- [3] Yazici, S., Inan, G., Tabak, V.: Effect of aspect ratio and volume fraction of steel fiber on the mechanical properties of SFRC, *Construction and Building Materials*, 21 (2007) 6, pp. 1250-1253, <http://dx.doi.org/10.1016/j.conbuildmat.2006.05.025>
- [4] Michels, J., Christen, R., Waldmann, D.: Experimental and numerical investigation on postcracking behavior of steel fiber reinforced concrete, *Engineering Fracture Mechanics*, 98 (2013) 1, pp. 326-349, <http://dx.doi.org/10.1016/j.engfracmech.2012.11.004>
- [5] Soulioti, D., Barkoula, N.M., Paipetis, A., Matikas, T.E., Shiotani, T., Aggelis, D.G.: Acoustic emission behavior of steel fibre reinforced concrete under bending, *Construction and Building Materials*, 23 (2009) 12, pp. 3532-3536, <http://dx.doi.org/10.1016/j.conbuildmat.2009.06.042>
- [6] Soulioti, D.V., Barkoula, N.M., Paipetis, A., Matikas, T.E.: Effects of fibre geometry and volume fraction on the flexural behaviour of steel-fibre reinforced concrete, *Strain* 47 (SUPPL. 1):e535-e541, 2011, <http://dx.doi.org/10.1111/j.1475-1305.2009.00652.x>
- [7] Bencardino, F., Rizzuti, L., Spadea, G., Swamy, R.N.: Experimental evaluation of fiber reinforced concrete fracture properties, *Composites Part B, Engineering*, 41 (2005) 1, pp. 17-24, <http://dx.doi.org/10.1016/j.compositesb.2009.09.002>
- [8] Caggiano, A., Cremona, M., Faella, C., Lima, C., Martinelli, E.: Fracture behavior of concrete beams reinforced with mixed long/short steel fibers, *Construction and Building Materials*, 37 (2012), pp. 832-840, <http://dx.doi.org/10.1016/j.conbuildmat.2012.07.060>
- [9] Köksal, F., Sahin, Y., Gencil, O., Yiğit, T.: Fracture energy-based optimisation of steel fibre reinforced concretes, *Engineering Fracture Mechanics*, 107 (2013), pp. 29-37, <http://dx.doi.org/10.1016/j.engfracmech.2013.04.018>
- [10] Balaguru, P., Narahar, R., Patel, M.: Flexural toughness of steel fiber reinforced concrete, *ACI Materials Journal*, 89 (1992) 6, pp. 541-546
- [11] Hughes, B.P., Fattuhi, N.I.: Workability of steel-fibre-reinforced concrete, *Magazine of Concrete Research*, 28 (1976) 96, pp. 157-161, <http://dx.doi.org/10.1680/mac.1976.28.96.157>
- [12] Orbe, A., Cuadrado, J., Losada, R., Rojí, E.: Framework for the design and analysis of steel fiber reinforced self-compacting concrete structures, *Construction and Building Materials*, 35 (2012), pp. 676-686, <http://dx.doi.org/10.1016/j.conbuildmat.2012.04.135>
- [13] Cunha, V.M.C.F., Barros, J.A.O., Sena-Cruz, J.M.: Pullout behavior of steel fibers in self-compacting concrete, *Journal of Materials in Civil Engineering*, 22 (2010) 1, pp. 1-9, [http://dx.doi.org/10.1061/\(ASCE\)MT.1943-5533.0000001](http://dx.doi.org/10.1061/(ASCE)MT.1943-5533.0000001)
- [14] Dupont, D., Vandewalle, L.: Distribution of steel fibres in rectangular sections, *Cement and Concrete Composites*, 27 (2005) 3, pp. 391-398, <http://dx.doi.org/10.1016/j.cemconcomp.2004.03.005>
- [15] Laranjeira, F., Aguado, A., Molins, C., Grünwald, S., Walraven, J., Cavalaro, S.: Framework to predict the orientation of fibers in FRC, A novel philosophy, *Cement and Concrete Research*, 42 (2012) 6, pp. 752-768, <http://dx.doi.org/10.1016/j.cemconres.2012.02.013>
- [16] Laranjeira, F., Grünwald, S., Walraven, J., Blom, C., Molins, C., Aguado, A.: Characterization of the orientation profile of steel fiber reinforced concrete, *Materials and Structures/Materiaux et Constructions*, 44 (2011) 6, pp. 1093-1111, <http://dx.doi.org/10.1617/s11527-010-9686-5>
- [17] Soroushian, P., Lee, C.D.: Distribution and orientation of fibers in steel fiber reinforced concrete. *ACI Materials Journal*, 87 (1990) 5, pp. 433-439.
- [18] Barragán, B.E., Gettu, R., Martín, M.A., Zerbino, R.L.: Uniaxial tension test for steel fibre reinforced concrete - A parametric study, *Cement and Concrete Composites*, 25 (2003) 7, pp. 767-777, [http://dx.doi.org/10.1016/S0958-9465\(02\)00096-3](http://dx.doi.org/10.1016/S0958-9465(02)00096-3)
- [19] US Patent 6740282B1 USPN: Method and device for magnetskik alignment of fibres, 2004.
- [20] Robins, P.J., Austin, S.A., Jones, P.A.: Spatial distribution of steel fibres in sprayed and cast concrete, *Magazine of Concrete Research*, 55 (2003) 5, pp. 225-235, <http://dx.doi.org/10.1680/mac.2003.55.3.225>
- [21] CinkarnaCelje, <http://www.cinkarna.si/en/products/>, 2014.
- [22] KrampeHarex, www.krampeharex.com, 2014.
- [23] Schnell, J., Schladitz, K., Schuler, F.: Direction Analysis of Fibres in Concrete on Basis of Computed Tomography, *Beton- und Stahlbetonbau*, 105 (2010) 2, pp. 72-77, <http://dx.doi.org/10.1002/best.200900055>
- [24] Wuest, J., Denarié, E., Brühwiler, E., Tamarit, L., Kocher, M., Gallucci, E.: Tomography analysis of fiber distribution and orientation in ultra high-performance fiberreinforced composites with high-fiber dosages, *Experimental Techniques*, 33 (2009) 5, pp. 50-55, <http://dx.doi.org/10.1111/j.1747-1567.2008.00420.x>
- [25] Czaderski, C., Soudki, K., Motavalli, M.: Front and side view image correlation measurements on FRP to concrete pull-off bond tests, *Journal of Composites for Construction* 14 (2010) 4, pp. 451-463, [http://dx.doi.org/10.1061/\(ASCE\)CC.1943-5614.0000106](http://dx.doi.org/10.1061/(ASCE)CC.1943-5614.0000106)
- [26] Michels, J., Czaderski, C., El-Hacha, R., Brönnimann, R., Motavalli, M.: Temporary bond strength of partly cured epoxy adhesive for anchoring prestressed CFRP strips on concrete, *Composite Structures*, 94 (2012) 9, pp. 2667-2676, <http://dx.doi.org/10.1016/j.engfracmech.2011.04.008>
- [27] Denneman, E., Wu, R., Kearsley, E.P., Visser, A.T.: Discrete fracture in high performance fibre reinforced concrete materials, *Engineering Fracture Mechanics*, 78 (2011) 10, pp. 2235-2245
- [28] Bazant, Z.P., Planas, J.: Fracture and Size Effect in Concrete and other Quasibrittle Materials, CRC Press, 1997.
- [29] Elices, M., Guinea, G.V., Planas, J.: Measurement of the fracture energy using three-point bend tests, Part 3-influence of cutting the P- δ tail, *Materials and Structures*, 25 (1992) 6, pp. 327-334, <http://dx.doi.org/10.1007/BF02472591>
- [30] Elices, M., Guinea, G.V., Planas, J.: On the measurement of concrete fracture energy using three-point bend tests, *Materials and Structures/Materiaux et Constructions*, 30 (1997) 200, pp. 375-376, <http://dx.doi.org/10.1007/bf02480689>
- [31] DBV: Merkblatt Stahlfaserbeton, 2001.
- [32] Barr, B.I.G., Lee, M.K., De Place Hansen, E.J., Dupont, D., Erdem, E., Schaeerlaekens, S., Schnütgen, B., Stang, H., Vandewalle, L.: Round-robin analysis of the RILEM TC 162-TDF beam-bending test, Part 1 - Test method evaluation, *Materials and Structures/Materiaux et Constructions*, 36 (2003) 263, pp. 609-620, <http://dx.doi.org/10.1007/bf02483281>
- [33] CNR: Guide for the Design and Construction of Fiber-Reinforced Concrete Structures, Italy, 2007.